

Formation of the Cameroon Volcanic Line by lithospheric basal erosion: Insight from mantle seismic anisotropy



A.A. Elsheikh*, S.S. Gao, K.H. Liu

Department of Geosciences and Geological and Petroleum Engineering, Missouri University of Science and Technology, Rolla, MO 65409, USA

ARTICLE INFO

Article history:

Received 26 December 2013
Received in revised form 13 June 2014
Accepted 15 June 2014
Available online 27 June 2014

Keywords:

Shear-wave splitting
Cameroon Volcanic Line
Intraplate volcanic segments
Lithospheric channel

ABSTRACT

The formation mechanism of intraplate volcanism such as that along the Cameroon Volcanic Line (CVL) is one of the controversial problems in global tectonics. Models proposed by previous studies include re-activation of ancient suture zones, lithospheric thinning by mantle plumes, and edge-driven mantle convection. To provide additional constraints on the models for the formation of the CVL, we measured shear-wave splitting parameters at 36 stations in the vicinity of the CVL using a robust procedure involving automatic batch processing and manual screening to reliably assess and objectively rank shear-wave splitting parameters (fast polarization directions and splitting times). The resulting 432 pairs of splitting parameters show a systematic spatial variation. Most of the measurements with ray-piercing points (at 200 km depth) beneath the CVL show a fast direction that is parallel to the volcanic line, while the fast directions along the coastline are parallel to the continental margin. The observations can best be interpreted using a model that involves a channel flow at the bottom of the lithosphere originated from the NE-ward movement of the asthenosphere relative to the African plate. We hypothesize that progressive thinning of the lithosphere through basal erosion by the flow leads to decompression melting and is responsible for the formation of the CVL. The model is consistent with the lack of age progression of the volcanoes in the CVL, can explain the formation of both the continental and oceanic sections of the CVL, and is supported by previous geophysical observations and geodynamic modeling results.

© 2014 Elsevier Ltd. All rights reserved.

1. Introduction

Most of the Earth's magmatism is associated with dehydration of minerals in subducting slabs and with decompression melting along mid-ocean ridges, and thus can be well-explained by the theory of plate tectonics (e.g., Turcotte and Oxburgh, 1978; Courtillot et al., 2003). The formation mechanism for intraplate magmatism, on the other hand, remains enigmatic. Various models have been proposed to explain intraplate magmatism, including those involving mantle plumes (Morgan, 1972; Courtillot et al., 2003), tensional cracking in the lithosphere (Turcotte and Oxburgh, 1978; Anderson, 2000), and edge-driven convection (EDC) (King and Anderson, 1998).

The African plate is ideal for studying intraplate magmatism. It contains several intraplate volcanic segments or centers that are remote from the African plate boundaries (Fig. 1). One of such segments is the NE–SW oriented Cameroon Volcanic Line (CVL), which consists of a continental and an oceanic section. The CVL intercepts

with the Atlantic coastline at the joint point between the E–W and N–S segments of the coastline (Fig. 2).

Many studies proposed that the CVL was the result of the NE-ward movement of the African plate over a mantle plume that is currently beneath St. Helena (e.g., Morgan, 1983) (Fig. 1). This model predicts that the age of the volcanoes decreases toward the SW. Such an age progression, however, is not observed (e.g., Fitton and Dunlop, 1985). Additionally, $^3\text{He}/^4\text{He}$ ratios measured along the CVL are lower than those observed at typical hotspots such as Loihi and Iceland (Aka et al., 2004), probably suggesting an upper-mantle origin of the magmatism. Other studies concluded that the CVL was due to decompression melting beneath re-activated shear zones on the African continent (e.g., Fairhead, 1988). This model, while can explain the lack of age progression, cannot satisfactorily explain the existence of the oceanic section of the CVL. The third group of studies advocated edge-driven convection as the major cause of the CVL (King and Ritsema, 2000; Koch et al., 2012; Milelli et al., 2012). This model suggests that the upwelling flow thins the lithosphere and creates a line of volcanoes parallel to the boundary between two areas with contrasting lithospheric thickness. In the study area, the northern edge of the Congo craton is a potential locale for the EDC to occur and thus

* Corresponding author. Tel.: +1 5733414058; fax: +1 5733416935.

E-mail addresses: aaer4c@mst.edu (A.A. Elsheikh), sgao@mst.edu (S.S. Gao), liukh@mst.edu (K.H. Liu).

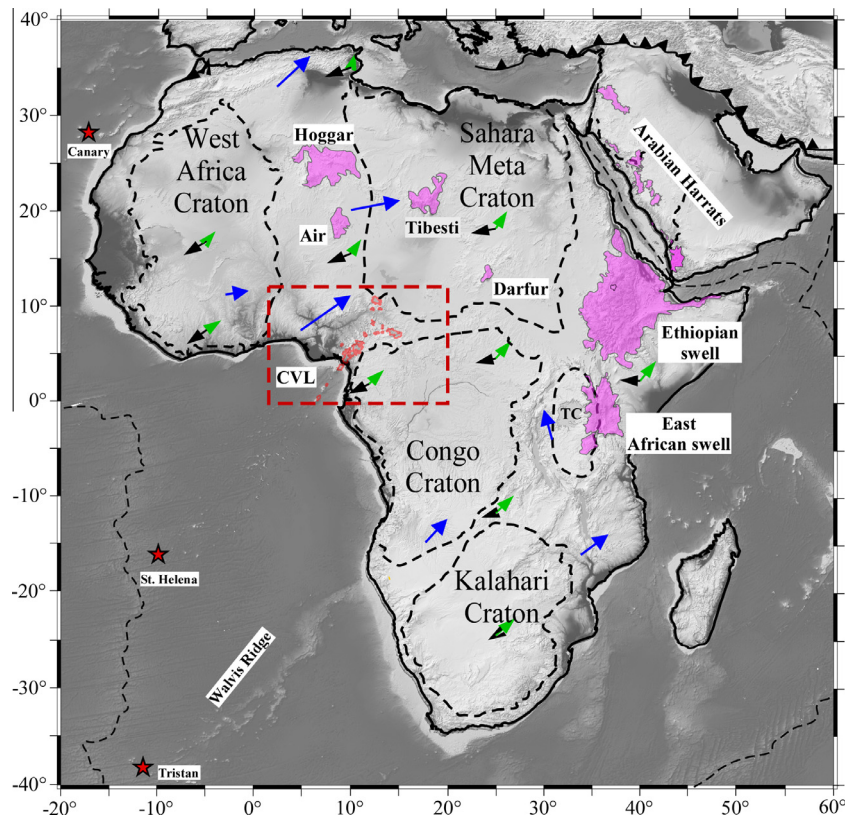


Fig. 1. Topographic relief map of Africa showing major intraplate volcanic centers and cratons (Turcotte and Oxburgh, 1978; Abdelsalam et al., 2011). CVL, Cameroon Volcanic Line. TC, Tanzania Craton. The area inside the red dashed rectangle is shown in Figs. 2 and 3. The green arrows represent absolute plate motion (APM) vectors calculated using the GMHRF model (Dubrovine et al., 2012), and the black arrows show APM vectors determined by the HS3-NUVEL1A model (Gripp and Gordon, 2002). The blue arrows indicate the horizontal component of mantle flow predicted at 250 km depth (Forte et al., 2010). Red stars represent the locations of the Atlantic mantle plumes (Dubrovine et al., 2012). (For interpretation of the references to color in this figure legend, the reader is referred to the web version of this article.)

could be responsible for the formation of the continental section of the CVL (Fig. 3). However, this model cannot explain the orientation of the zone of thinned oceanic lithosphere should be parallel to the coastline, while the actual CVL has a NE–SW strike. In addition, as described below, neither the plume nor the EDC model is supported by shear-wave splitting (SWS) measurements.

Splitting analysis of P-to-S converted phases at the core-mantle boundary on the receiver side, including the PKS, SKKS, and SKS (hereinafter collectively referred to as XKS) phases, is considered to be one of the most effective tools in measuring seismic anisotropy, which is mostly caused by deformational processes in the mantle (see Silver, 1996; Savage, 1999, and Fouch and Rondenay, 2006 for reviews). Numerous XKS splitting studies demonstrated that the spatial distribution of the two splitting parameters Φ , which is the polarization direction of the faster wave, and δt , the splitting time between the faster and slower waves, are crucial to understand mantle circulation patterns. The fast direction reflects the mantle deformation direction, while the splitting time quantifies the magnitude of the mantle deformation (Conrad and Behn, 2010; Kreemer, 2009).

The coefficient of anisotropy is defined as $(V_{\text{fast}} - V_{\text{slow}})/V_{\text{mean}}$ where V_{fast} and V_{slow} are the fast and slow shear-wave velocities, respectively and V_{mean} is the mean velocity (Birch, 1960; Wolfe and Solomon, 1998). The global average of the splitting time observed using teleseismic XKS waves is 1.0 s, which corresponds to a thickness of about 100 km for a 4% anisotropy (Silver, 1996). Olivine lattice-preferred orientations (LPO) likely forms as a result of dislocation creep deformation, leading to a macroscopic anisotropy in the upper mantle (e.g., McKenzie, 1979; Ribe, 1989; Fouch

and Rondenay, 2006; Conrad et al., 2007). Numerical modeling and experimental mineral physics studies indicate that under uniaxial compression, the olivine a -axis rotates to be orthogonal to the maximum compressional strain direction. Under pure shear, it becomes perpendicular to the shortening direction; and under progressive simple shear, it aligns parallel to the flow direction (Ribe and Yu, 1991; Chastel et al., 1993; Zhang and Karato, 1995; Savage, 1999; Liu, 2009). Therefore, the fast direction may reveal the flow direction in the asthenosphere as observed in ocean basins, continental rifts, and passive margins (Wolfe and Solomon, 1998; Gao et al., 1994, 1997, 2008, 2010; Refayee et al., 2013).

In the lithosphere, Φ is primarily parallel to the trend of past tectonic events, as revealed at numerous locales (McNamara et al., 1994; Liu et al., 1995; Silver, 1996; Barruol and Hoffmann, 1999; Fouch and Rondenay, 2006; Li and Chen, 2006; Liu, 2009). In addition, vertical magmatic dikes in the lithosphere can result in XKS splitting with a fast direction parallel to the main strike direction of the dikes (Gao et al., 1997, 2010). This mechanism was suggested to explain rift-parallel fast directions detected in active continental rifts such as the Baikal rift zone (Gao et al., 1997), the East African rift system (Gao et al., 1997, 2010; Kendall et al., 2005), and failed rifts such as the southern Oklahoma aulacogen (Gao et al., 2008).

2. Geophysical background

The CVL is an ~ 1600 km elongated Y-shaped feature of Cenozoic volcanoes (e.g., Fitton, 1987; Aka et al., 2004; Tokam et al., 2010; Reusch et al., 2010; Milelli et al., 2012) (Fig. 3). It is

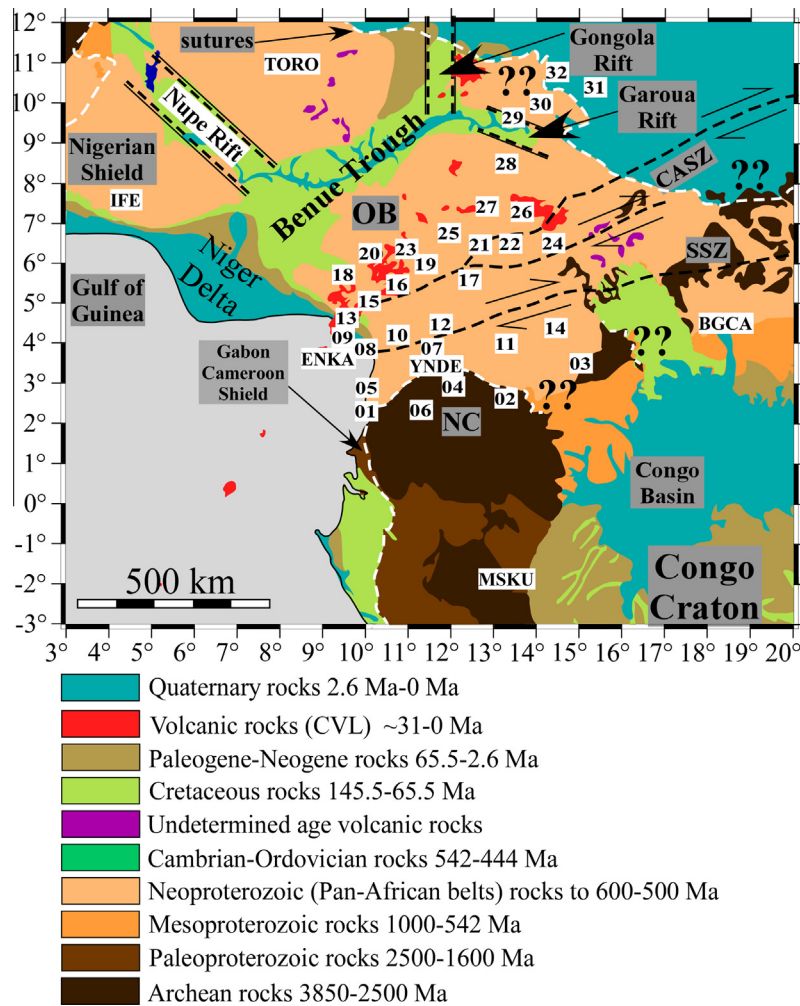


Fig. 2. Major tectonic elements of western and central Africa showing main geological subdivision units (International Geological Map of Africa, 1990). The white squares and rectangles show seismic stations used in the study.

located between the Congo craton to the south and the Oubangui Belt to the north, which was created by the collision between four different terranes including the São Francisco and Congo cratons, the West African craton, and a Pan-African mobile domain during the formation of the Gondwana (e.g., [Castaing et al., 1994](#); [Toteu et al., 2004](#); [Begg et al., 2009](#); [Tokam et al., 2010](#)). The land section of the CVL includes several major volcanoes such as Mounts Cameroon, Manengouba, Bambouto, and Oku, and extends from the Gulf of Guinea all the way to the Chad frontier (e.g., [Aka et al., 2004](#)) (Fig. 3). The oceanic section includes the islands of Annobon (formerly called Pagalu), São Tomé, Príncipe, and Bioko (Fig. 3). The Pan-African basement rocks almost cover the entire continental portion of the CVL with more than 60 anorogenic ring complexes exposed on the surface of the continental section of the CVL. The majority of these ring complexes are concentrated in the southwestern part of the continental section. The basement rocks exposed on the CVL are mainly alkaline (basalts, basanites, trachytes, and phonolites) with the exception of the nephelinitic lava that erupted near Mt. Etinde ([Fitton and Hughes, 1981](#); [Fitton, 1987](#); [Lee et al., 1994](#); [Aka et al., 2004](#); [Deruelle et al., 1991, 2007](#)).

Nearly all of the global and regional tomographic models agree that the CVL is underlain by upper mantle low-velocity anomalies, while the Congo and West Africa cratons are underlain by high-velocity anomalies (e.g., [King and Ritsema, 2000](#); [Ritsema and](#)

[van Heijst, 2000](#); [Priestley et al., 2008](#); [Reusch et al., 2010](#)). However, the lateral and depth extent of the upper mantle low-velocity anomalies beneath the CVL, which plays an important role for understanding the origin of the CVL, is still a subject of considerable debate (e.g., [Reusch et al., 2010](#)). [King and Ritsema \(2000\)](#) used numerical modeling constrained by seismic tomography results to understand the origin of African and South American intraplate volcanisms. They found relatively high seismic shear-wave velocities in the mantle transition zone beneath the Congo and West African cratons and suggested that EDC from beneath the Congo craton is responsible for the formation of the CVL.

On a local scale, [Dorbath et al. \(1986\)](#) performed inversion of teleseismic P-wave travel-time residuals across the Adamawa Plateau and the central African shear zone (CASZ) in central Cameroon (Fig. 3). They revealed a low-velocity anomaly beneath the Adamawa Plateau striking ENE at the depth of ~190 km. [Plomerova et al. \(1993\)](#) examined the lithospheric thickness and anisotropy within the upper mantle in the Adamawa Plateau using teleseismic.

P- and PKP-arrival times recorded by a network of 40 seismic stations deployed along the plateau. They concluded that a thinned lithosphere and a 2% low-velocity anomaly beneath the CASZ in Cameroon are caused by mantle upwelling. The most recent tomographic imaging using body-waves shows a tabular low-velocity anomaly beneath the CVL with a depth extension not less than 300 km ([Reusch et al., 2010](#)). They argued that the low-velocity

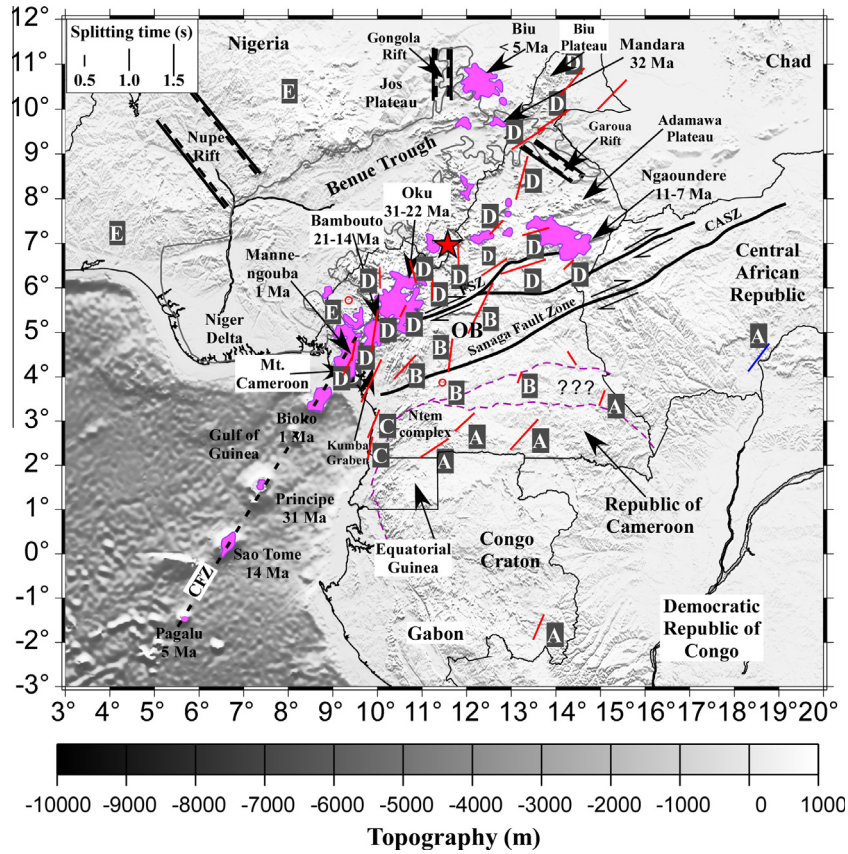


Fig. 3. A map of the study area showing locations and ages of the Cameroon Volcanic Line (magenta features) (Fitton and Dunlop, 1985; Fitton, 1987) and previous shear-wave splitting measurements (red and blue bars). The orientation of the bars represents the fast direction, the length is proportional to the splitting time, and red circles represent null measurements. The blue bar near the right edge of the figure represents the measurement from Barruol and Ismail (2001), and the red bars and circles represent measurements from Koch et al. (2012). FSZ, Foubman Shear Zone. CASZ, Central African Shear Zone. CFZ, Cameroon Fracture Zone (Meyers et al., 1998; Reusch et al., 2010). OB, Oubanguides Belt. The dashed magenta line represents the northern edge of the Congo craton (Schlüter, 2006; Reusch et al., 2010). The red star shows the location of the Cameroon mantle plume (Burke, 2001). The letters in the rectangles indicate the name of the sub-area that the stations belong to (see Section 5.1). (For interpretation of the references to color in this figure legend, the reader is referred to the web version of this article.)

anomaly beneath the CVL is consistent with a model involving EDC along the northern boundary of the Congo craton.

Many studies have analyzed crustal structure beneath the study area using a variety of techniques including active and passive seismic source analysis (e.g., Stuart et al., 1985; Dorbath et al., 1986; Tabod et al., 1992; Plomerova et al., 1993; Sandvol et al., 1998; Hansen et al., 2009; Obrebski et al., 2010; Tokam et al., 2010; Gallacher and Bastow, 2012) and gravity studies (e.g., Fairhead and Okereke, 1987; Djomani et al., 1995; Nnange et al., 2000; Toteu et al., 2004; Tadjou et al., 2009). Tokam et al. (2010) used data from the Cameroon Broadband Seismic Experiment (CBSE) network, which consisted of 32 portable broad-band seismometers deployed between January 2005 and February 2007 across Cameroon, to investigate crustal structure beneath the CVL by utilizing P-wave receiver functions (RFs) and surface wave dispersion data. They found a thin crust of 26–31 km in thickness beneath the Garoua rift and the coastal plain (Fig. 3), and a thicker crust of 43–48 km with a mafic lower crust beneath the Congo craton. The crustal thickness in the CVL and the Oubanguides Belt varies between 35 and 39 km (Fig. 3). They suggested that the thin crust beneath the coastal plain is caused by the opening of the southern Atlantic Ocean, while the formation of the Benue Trough in the early Cretaceous thinned the crust in the Garoua rift. The thicker crust in the Congo craton was formed as a result of continent–continent collision in the development of the Gondwana. Recently, Gallacher and Bastow (2012) applied a RFs stacking technique (Zhu and Kanamori, 2000) using the CBSE data to study

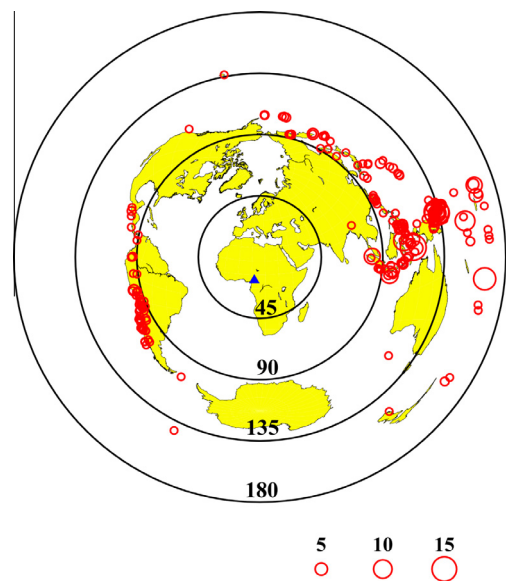


Fig. 4. An azimuthal equidistant projection map of the Earth showing the distribution of earthquakes used in the study (open dots). The radius of the dots is proportional to the number of resulting well-defined splitting measurements from the events. Circles and corresponding labels show the distance (in degree) to the center of the study area.

crustal structure beneath the CVL. Most of the crustal thickness measurements by Gallacher and Bastow (2012) are comparable with those obtained by Tokam et al. (2010).

3. Previous seismic anisotropy studies

During the past two decades, XKS splitting studies provided important constraints on various models for the formation, structure, and dynamics of various Cenozoic tectonic processes on the African plate including rifting, uplifting, volcanism, and lithosphere deformation (e.g., Vinnik et al., 1989; Gao et al., 1997, 2010; Barruol and Hoffmann, 1999; Silver et al., 2001; Barruol and Ismail, 2001; Gashawbeza et al., 2004; Walker et al., 2004; Kendall et al., 2005, 2006; Bagley and Nyblade, 2013; Elsheikh et al., 2014). In our study area, Chevrot (2000) conducted multi-channel SKS splitting analysis to constrain seismic anisotropy beneath station BGCA (formerly called BNG). He suggested that the splitting parameters $\Phi = 17 \pm 1.0^\circ$ and $\delta t = 0.74 \pm 0.03$ s observed at the station are due to the present-day movement of the African plate. For the same station, Barruol and Hoffmann (1999) found $\Phi = 29 \pm 4.0^\circ$ and $\delta t = 0.84 \pm 0.11$ s. Barruol and Ismail (2001) investigated upper mantle anisotropy beneath the African plate using data from the Incorporated Research Institutions for Seismology (IRIS) and GEOSCOPE stations including

BGCA. They obtained a fast direction of $35 \pm 2.0^\circ$ and a splitting time of 0.79 ± 0.06 s at BGCA.

Koch et al. (2012) reported station-averaged SKS and SKKS splitting parameters beneath Cameroon (Fig. 3) using data from the CBSE and station MSKU. The study also used SWS results at station BGCA from Barruol and Ismail (2001). They identified four regions with different splitting parameters. The Congo craton and the Garoua rift have NE–SW fast directions and splitting times of about 1.0 s. Spatially varying fast directions and splitting times as small as 0.3 s are observed at the northern edge of the Congo craton and in the area between the CVL and the craton in central Cameroon (Fig. 3). Along the CVL, the mean fast direction is about 30° , and the splitting times are 0.7 s. They suggested that the observed anisotropy beneath central and northeast Cameroon is associated with fossil anisotropy due to past collisional events, while most of the observed anisotropy beneath the CVL is related to EDC originated from variations in temperature between the Congo craton and the mobile belts that flank the northern boundary of the Congo craton (e.g., King and Anderson, 1995, 1998; King and Ritsema, 2000; Koch et al., 2012) (Fig. 3). According to this model, the hotter materials beneath the Congo cratonic root propagate northward to the mobile belts, leading to mostly N–S fast directions in the CVL. De Plaen et al. (2014) also used data from the CBSE stations to study seismic anisotropy beneath Cameroon via analysis of XKS

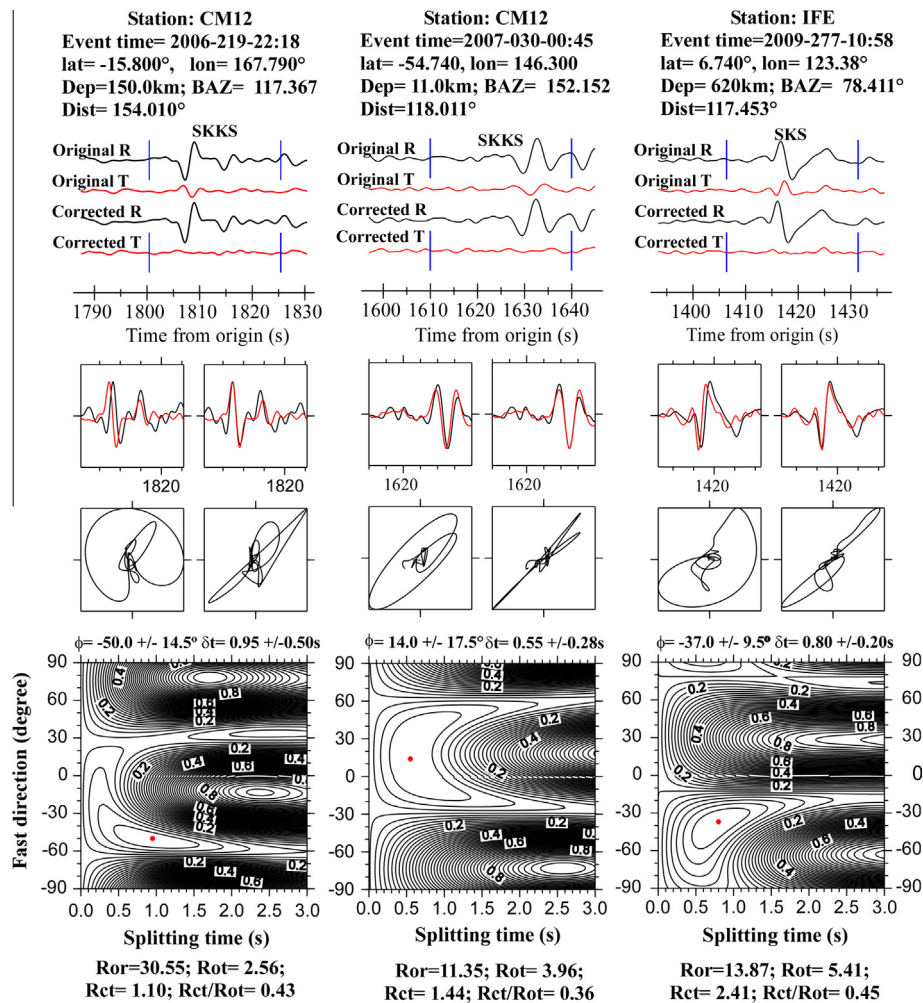


Fig. 5. Original and corrected SKS seismograms, particle motion patterns, and contour map of the error function for events recorded by stations CM12 and IFE, respectively. The red dot in Fig. 5 (bottom) marks the optimal splitting parameters. (For interpretation of the references to color in this figure legend, the reader is referred to the web version of this article.)

splitting. They reported NNE–ENE fast directions with splitting time varies from 0.48 to 1.95 s in Cameroon. They concluded that the observed anisotropy in Cameroon was related to frozen anisotropy developed as a result of Cretaceous rifting in the Gondwana supercontinent.

In this study, we take the advantage of the recently released broadband seismic data in a larger area surrounding the CVL than that in previous studies, including data from Cameroon, the Central African Republic, Gabon, and Nigeria, to provide additional constraints on the origin of the CVL. We conclude that SWS results favor a model that involves a lithospheric channel that developed as a result of gradual basal erosion by the underlying asthenosphere on the northern edge of the Congo craton. This mechanism in turn causes decompression melting and is responsible for the formation of both the continental and oceanic sections of the CVL.

4. Data and methods

We use all the broadband XKS data recorded in the study area and archived until early 2013 at IRIS Data Management Center (DMC). The seismic events were selected based on the following criteria: For PKS, the epicentral distance range is 120–180°, and the cutoff magnitude is 5.8; for SKKS, the corresponding values are 95–180° and 5.6; and for SKS, they are 84–180 and 5.6. In order to take the advantage of the sharper waveforms for all the PKS, SKKS, and SKS phases from deeper events, the cutoff magnitude is reduced by 0.1 unit for events with a focal depth equal or greater than 100 km (Liu and Gao, 2013). Fig. 4 shows the distribution of the 204 events that produced at least one well-defined measurement. The majority of the events are located in the western Pacific and Nazca subduction zones. Thirty-six stations were found to produce at least one well-defined XKS splitting measurement. One of the stations used in this study, BGCA in Central Africa, belongs to GEOSCOPE. This station has been operating since June 1994. Stations EKNA, IFE, and YNDE are part of the African Array, while station TORO is a Nigerian National Seismic Network station. In addition, we used data from station MSKU, which belongs to IRIS/USGS Global Seismographic Network in Masuku Gabon. This station has been operating since March 1999. The rest of the stations are from the CBSE (Tokam et al., 2010). During our shear-wave-splitting analysis, we detected and corrected a misidentification of the vertical and E–W components at station IFE.

This study used a procedure for measuring and objectively ranking XKS splitting parameters based on the minimization of transverse energy method (Silver and Chan, 1991; Liu et al., 2008; Gao and Liu, 2009; Liu, 2009; Gao et al., 2010; Liu and Gao, 2013). The seismograms were band-pass filtered in the 0.04–0.5 Hz range which is the most effective frequency band for enhancing the signal-to-noise ratio (S/N). The optimal XKS time window is visually verified and adjusted if necessary to exclude non-XKS arrivals (Liu and Gao, 2013). The uncertainties in the measurements are calculated based on the inverse *F*-test (Silver and Chan, 1991).

Fig. 5 shows examples of the original and corrected waveforms and their particle motion diagrams. The quality of the resulting measurements are ranked using the S/N on the original radial (R_{or}), original transverse (R_{ot}), and corrected transverse (R_{ct}) components (Liu et al., 2008). We classified a measurement as a quality A measurement when $R_{or} \geq 10.0$, $R_{ot} \geq 2.0$, and $R_{ct}/R_{ot} \leq 0.7$, that is, outstanding energy on both the radial and transverse components is observed, and the resulting parameters were effective in reducing the energy on the transverse component (Liu et al., 2008). For a quality B event, the corresponding values are $3.0 \leq R_{or} < 10.0$, $R_{ot} \geq 2.0$, and $R_{ct}/R_{ot} \leq 0.7$. The ranking was manually screened and adjusted if necessary.

5. Results

A total of 432 pairs of quality A or B measurements were obtained after manual screening of the results (Fig. 6). In addition, we observed null measurements at almost all of the stations. Null measurements are characterized by the lack of observable energy on the transverse component as a result of the backazimuth (BAZ) directions being either parallel or perpendicular to the fast direction, or the media traveled by the XKS phase is isotropic (e.g., Silver and Chan, 1991; Liu and Gao, 2013). Two or more null events with non-parallel or orthogonal back-azimuths indicate the paucity of anisotropy. Our results demonstrate that clear splitting is observed at all stations in the study area, and thus the null measurements are not used in the discussions below.

5.1. Spatial variations of SWS measurements

We divide the CVL and the adjacent regions into five sub-areas based on the characteristics of the SWS measurements and also on different tectonic provinces (Figs. 2 and 3). Area A is on the Congo craton and includes stations CM02, 03, 04, 06, BGCA and MSKU and contains 208 pairs of SWS measurements. The mean fast direction in this area $44.4 \pm 20^\circ$, and the mean splitting time is 0.91 ± 0.29 s. Area B lies on the northern edge of the Congo craton and includes stations CM07, 10, 11, 12, 17, and YNDE, possessing 40 pairs of SWS measurements. The mean fast direction is $22 \pm 28^\circ$, and the mean splitting time is 1.17 ± 0.40 s. This area also includes stations CM08 and CM14, but data from these stations cannot be used for SWS analysis due to the lack of high-quality waveforms. Area C, the area along the Cameroon shoreline, consists of stations CM01 and 05 and contains 10 pairs of SWS measurements with a mean fast direction of $44 \pm 22^\circ$ and a mean splitting time of 0.7 ± 0.2 s. Area D is the main part of the CVL and spans from southern Cameroon to the Chad border, and includes stations EKNA, CM09, 13, 15, 16, and CM19–CM32 with 156 pairs of SWS measurements. Within Area D, we observed a mean fast direction of $53.3 \pm 20.7^\circ$, which is parallel to the general strike of the CVL, and a mean splitting time of 1.0 ± 0.32 s. Area E consists of stations IFE, TORO, and CM18 (Figs. 2 and 3). These stations are located in Nigeria and western Cameroon, wherein we observed a mean fast direction of $-55.9 \pm 15.9^\circ$ and a mean splitting time of 1.3 ± 0.39 s from 17 pairs of SWS measurements. The fast directions observed in Area E are mostly sub-parallel to the African coastline.

We next examine azimuthal variations of the observed splitting parameters, which are diagnostics of complex anisotropy (Silver and Savage, 1994). None of the stations shows periodic variations, suggesting that a single layer of anisotropy with a horizontal axis of symmetry is sufficient to explain the observations. There is, however, piercing-point dependence of the splitting parameters. For instance, at CM12, two events with a BAZ of 117° and 152° , respectively, shows a fast direction of -50° and 14° , respectively (Fig. 6), and nearly N–S fast directions were obtained from events with a BAZ of 26° and 66° , respectively. Similarly, at CM20, we observed fast directions of 15° and 62° for events with a BAZ of 28° and 81° , respectively. In general, measurements with ray-piercing points (at 200 km depth) beneath the CVL have a fast direction that is parallel to the CVL.

5.2. Comparison with previous results

To compare results from this study with station-averaged results of previous studies, we calculate the circular mean of the fast direction and the simple mean of the splitting times for each of the stations (Table 1). The major difference between our and previous results is that our splitting times are about twice as large

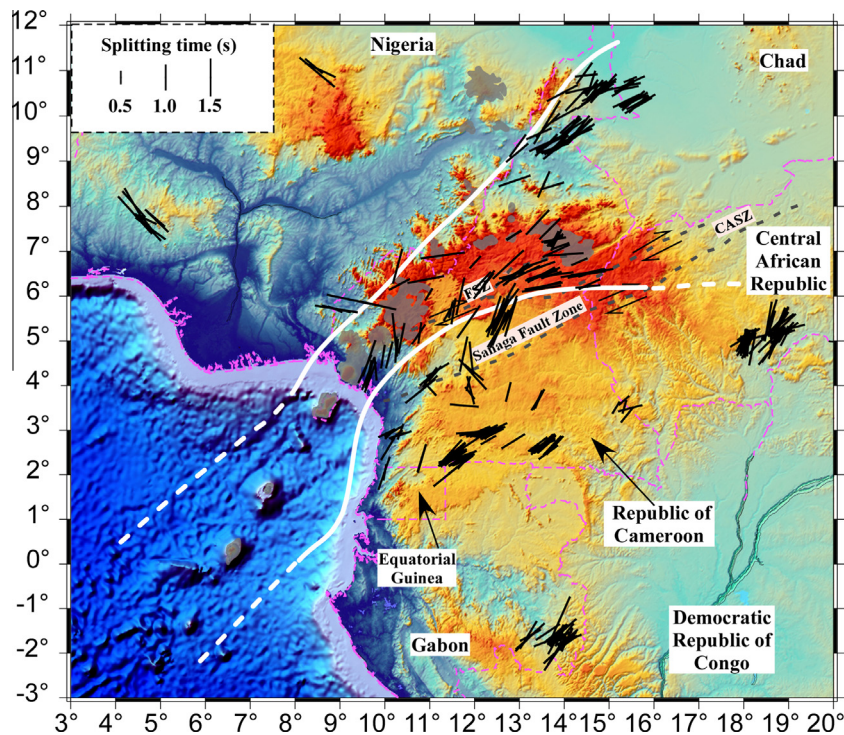


Fig. 6. Resulting XKS splitting parameters plotted above ray-piercing points at the depth of 200 km (black bars). The color image in the background shows the topographic relief of the study area. The white lines represent the boundary of the low-velocity zone at the depth of 200 km (Reusch et al., 2010). The dashed gray lines represent sutures (see Fig. 3). (For interpretation of the references to color in this figure legend, the reader is referred to the web version of this article.)

Table 1
Station locations and station-averaged splitting parameters.

Area	Station	Lat.	Long.	Φ	STD Φ	δt	STD δt	Number of measurements
A	BGCA	5.18	18.42	25.85	19.53	0.95	0.04	73
	CM02	2.7	13.29	53.04	7.05	0.98	0.02	17
	CM03	3.52	15.03	40.94	19.93	0.63	0.09	5
	CM04	2.98	11.96	66.23	7.05	0.99	0.06	18
	CM06	2.38	11.27	52.32	10.84	0.91	0.04	43
	MSKU	-1.66	13.61	49.3	13.43	0.88	0.04	52
B	CM07	3.87	11.46	-42.32	26.36	0.85	0.15	4
	CM10	4.22	10.62	42.03	7.69	0.91	0.13	6
	CM11	3.98	13.19	24.69	5.86	0.78	0.02	6
	CM12	4.48	11.63	-5.42	39.88	1.13	0.15	6
	CM17	5.55	12.31	25.24	6	1.46	0.07	16
	YNDE	3.87	11.46	-33.5	0.5	1.7	0.25	2
C	CM01	2.39	9.83	14.5	4.51	0.98	0.38	2
	CM05	2.94	9.91	51.89	17.69	0.69	0.06	8
D	CM09	4.23	9.33	22.5	2.5	1.23	0.03	2
	CM13	4.59	9.46	10.5	8.78	1.06	0.07	5
	CM15	5.03	9.93	5.22	6.99	1.1	0.15	5
	CM16	5.48	10.57	21	13.23	0.85	0.05	2
	CM19	5.97	11.23	15.65	7.81	0.96	0.2	4
	CM20	6.22	10.05	38.5	25.06	1.15	0.25	2
	CM21	6.47	12.62	50.9	13.09	1.1	0.1	13
	CM22	6.48	13.27	72.15	5.83	1.24	0.08	13
	CM23	6.37	10.79	55	25.68	0.98	0.48	2
	CM24	6.52	14.29	78.21	6.34	1.27	0.11	13
	CM25	6.76	11.81	62	20.92	1.18	0.58	2
	CM26	7.26	13.55	52.91	15.5	0.78	0.06	15
	CM27	7.36	12.67	57.5	2.5	0.65	0	2
	CM28	8.47	13.24	58.15	23.56	1.1	0.12	3
	CM29	9.35	13.39	53.57	9.28	1.04	0.05	19
	CM30	9.76	13.95	47.67	9.59	1.2	0.09	16
CM31	10.33	15.26	61.06	8.01	0.98	0.05	19	
CM32	10.62	14.37	51.44	15.18	1.09	0.09	19	
EKNA	4.23	9.33	19	5	1.5	0.28	1	
E	CM18	5.72	9.35	-76.22	4.36	1.32	0.22	5
	IFE	7.55	4.46	-45.12	9.52	1.27	0.12	9
	TORO	10.99	8.12	-54.95	7.1	1.32	0.27	3

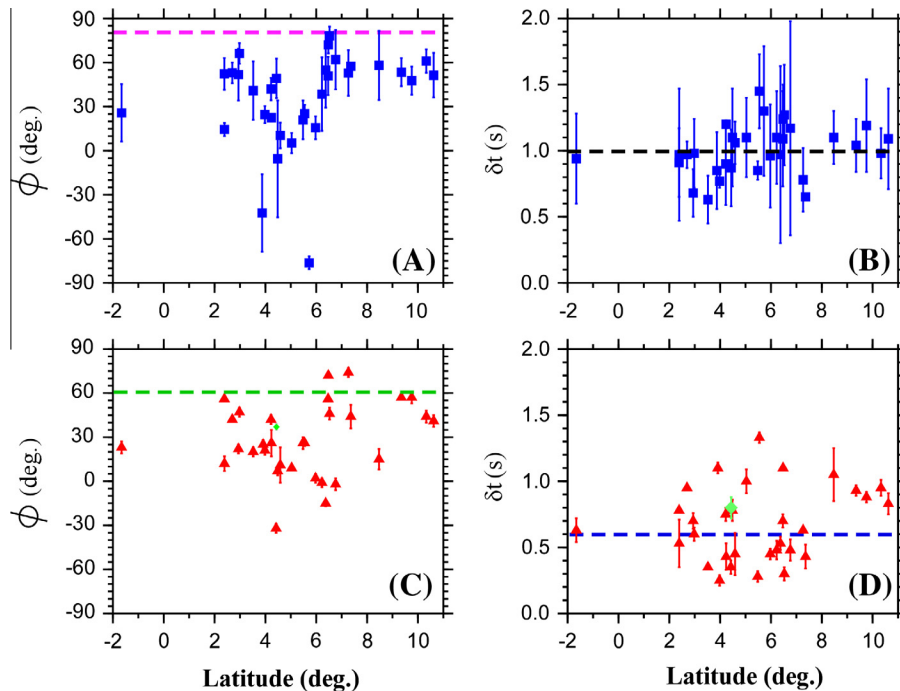


Fig. 7. Comparisons between our station-averaged measurements and those from previous studies. (A). Fast directions from this study plotted against the latitude. The dashed line shows the APM direction from the model of Gripp and Gordon (2002). (B). Splitting times from this study plotted against the latitude. The dashed line represents the average splitting time. (C). Fast directions from Barruol and Ismail (2001) (green diamond) and Koch et al. (2012) (red triangles) plotted against the latitude. The dashed line indicates the APM direction from the model of Doubrovine et al. (2012). (D). Splitting times obtained by Barruol and Ismail (2001) (green diamond) and Koch et al. (2012) (red triangles) plotted against the latitude. The dashed line shows the average splitting time observed by Koch et al. (2012). (For interpretation of the references to color in this figure legend, the reader is referred to the web version of this article.)

as those obtained by previous studies at almost all of the stations (Fig. 7). We hypothesize that this variation in splitting times is caused by the different method used by the studies. In addition to the obvious differences in most of the splitting time measurements between this and previous studies (Fig. 7), there are several other notable discrepancies. The first is that we did not use data from stations CM08 and CM14 due to equipment failures. CM08 did not yield sufficient data for our SWS analysis, while the N–S component at CM14 was not working (Tokam et al., 2010; Gallacher and Bastow, 2012), resulting in a nearly linear particle motion pattern (Liu and Gao, 2013). Using data from this station, Koch et al. (2012) obtained a fast direction of 25° and a splitting time of 1.1 s at station CM08. At CM14, they obtained a fast direction of -32° and a splitting time of 0.35 s. The second disagreement is that Koch et al. (2012) obtained null results at stations CM07 and CM18, but this study observed a mean fast direction of -42.3° and a mean splitting time of 0.9 ± 0.30 s at station CM07, and a fast direction of -76.2° and a splitting time of 1.3 ± 0.5 s at CM18. Third, at station CM20, we obtained a fast direction of 38° and a splitting time of 1.1 s while Koch et al. (2012) reported a fast direction of -1° and a splitting time of 0.48 s. Also, at station CM23, we observed a fast direction of 54.9° and a splitting time of 0.9 s while Koch et al. (2012) obtained a fast direction of -15° and a splitting time of 0.53 s. These discrepancies were mostly caused by the differences in the standards for data selection and result ranking, and the techniques used to obtain the results.

6. Discussion

In the cratonic environment, seismic anisotropy detectable by XKS splitting occurs either by LPO of crystallographic axes of anisotropic minerals (mainly olivine) developed under axis compression and simple shear, or shape-preferred orientation (SPO) formed by

preferably aligned vertical magmatic dikes. The former can either be resulted from shortening of the lithosphere or from flow in the asthenosphere, and the latter is mostly found in areas undergone extension (e.g., Nicolas and Christensen, 1987; Silver, 1996; Gao et al., 1997, 2010; Savage, 1999; Vauchez et al., 2000; Fouch and Rondenay, 2006; Nowacki et al., 2010; Refayee et al., 2013). In the following, we discuss each of the possibilities in light of the observed anisotropy and propose a model that explains both the SWS observations and the formation and evolution of the CVL.

6.1. Fossil anisotropy due to Precambrian collisional events

Many previous studies attributed observed anisotropy to lithospheric fabrics created by the last significant collisional tectonic events (e.g., Silver and Chan, 1991; Babuška and Plomerová, 1989; James and Assumpcao, 1996; McNamara et al., 1994; Silver, 1996; Fouch et al., 2004; Fouch and Rondenay, 2006). The observed anisotropy on the Kaapvaal and Zimbabwe cratons as well as on the Limpopo belt sandwiched between the cratons was considered as mostly the result of lithospheric fabrics (e.g., Silver et al., 2001; Barruol and Ismail, 2001; Fouch et al., 2004). Most of the study area lies between the Congo and West Africa cratons which consist of several tectonic shields including the Bomu-Kibalian, Nigerian, Gabon-Cameroon, and Man-Leo Shields developed during the Precambrian (e.g., Begg et al., 2009) (Figs. 2 and 3).

The N–S fast directions observed in the northern edge of the Congo craton (Area B) might originate from Precambrian collision events. These converging events include the collision between the Gabon-Cameroon Shield and the Bomu-Kibalian Shield to form the northern part of the Congo craton, and the collision between the Congo craton and the Oubanguides mobile belt (e.g., Castaing et al., 1994; Toteu et al., 2004; Begg et al., 2009). This speculation is in agreement with Koch et al. (2012) who suggested that measurements from the northern edge of the Congo craton represent

a fossil anisotropy resulted from Precambrian collisional events. However, most of our fast directions throughout the study area are aligned perpendicular to the suture zones (Figs. 3 and 6), and consequently, fossil seismic anisotropy, which has remained in the cratonic lithosphere since the Precambrian, cannot account for the majority of splitting parameters observed in the study.

6.2. Fossil anisotropy due to rifting of the Gondwana supercontinent

In areas of extended lithosphere such as continental extensional or rifting areas, the fast direction may align orthogonal to the extensional direction (Silver, 1996). This mechanism was employed to explain rift-parallel fast directions observed in the Main Ethiopian rift (Gashawbeza et al., 2004) and the Baikal and Kenya rifts (Gao et al., 1997). A recent study by De Plaen et al. (2014) suggested that the observed seismic anisotropy beneath the CVL was developed as a result of the rifting of the Gondwana supercontinent. While this model can explain the NE–SW fast directions in the CVL and adjacent areas (Figs. 2 and 6), an unusually large lithospheric anisotropy of about 9% is needed in order for the ~100 km thick lithosphere to produce the large (e.g., 1.95 s at CM12) splitting times. In addition, this model cannot account for the NE–SW fast directions observed at stations CM28–32 which are outside the ancient rifted zone (Fig. 2 and 6). If the anisotropy is originated in the lithosphere, these stations should have NW–SE fast directions parallel to the Garoua Rift and sutures (Fig. 2) which is not observed. Thus, fossil anisotropy resides in the lithosphere as a result of the rifting within the Gondwana supercontinent may not satisfactorily explain the observed anisotropy.

6.3. Mantle flow field associated with a mantle plume

Continental intraplate flood basalt development, uplifts, and bathymetric swells in Africa were often attributed to one or more mantle plumes (e.g., Morgan, 1972; Burke and Dewey, 1973; Nyblade and Robinson, 1994). Similarly, a mantle upwelling was proposed for the formation of the CVL (Van Houten, 1983; Morgan, 1983; Lee et al., 1994; Ebinger and Sleep, 1998; Burke, 2001). Burke (2001) suggested that a mantle plume, which is located at latitude 7°N and longitude 11.5°E (Fig. 3), could be responsible for the development of the CVL. Due to the upwelling of the plume material and the relative movement between the lithosphere and the asthenosphere, a parabolic flow pattern is expected in the vicinity of the plume, as observed in Hawaii and west-central Europe (Walker et al., 2001, 2005). Such a parabolic pattern is not observed (Fig. 6). Directly above a mantle plume, laboratory experiments suggest a complicated pattern of splitting parameters and small splitting times in the case of A-type olivine fabrics (Karato et al., 2008; Druken et al., 2013), which is not observed either. Therefore, our SWS results do not support an active plume beneath the CVL. This conclusion is consistent with the observation that the $^3\text{He}/^4\text{He}$ ratios measured on basaltic rocks along the CVL are lower than those observed at typical hotspots such as Loihi and Iceland (Aka et al., 2004). In addition, if a mantle plume is responsible for the formation of the CVL, the melt generation, as reflected by the expected higher-than-normal crustal V_p/V_s , should be much higher than what was observed beneath the CVL (Gallacher and Bastow, 2012). Thus, the mantle potential temperature beneath the CVL is significantly lower than that observed in Afar, Iceland, and other typical mantle plumes (Gallacher and Bastow, 2012). Body-wave seismic velocities observed beneath the CVL are also higher than those observed beneath the Ethiopia rift (Stuart et al., 1985; Bastow and Keir, 2011; Gallacher and Bastow, 2012). The absence of a deep mantle plume is also suggested by a nearly normal transition zone thickness (251 ± 10 km) observed beneath the CVL (Reusch et al., 2011).

6.4. Edge-driven convective flow

Geodynamic modeling suggests that variations in lithospheric thickness create a lateral contrast in temperature and viscosity near the top of the mantle, and the contrast may induce a small-scale convective mantle flow beneath the cratonic margin and could lead to uplifting, rifting, and formation of flood basalts (e.g., Anderson, 1994, 2001; King and Anderson, 1995, 1998; King and Ritsema, 2000; King, 2007).

The CVL is flanked by the Congo craton to the south and an area with thinner lithosphere to the north (Fig. 3), and thus is a preferable location for EDC with a flow direction that is approximately perpendicular to the CVL. Several studies (King and Ritsema, 2000; Reusch et al., 2010; Koch et al., 2012; Milelli et al., 2012) argued that this small-scale convection system is responsible for the formation of the CVL. This model can explain the lack of age progression along the CVL. However, the anticipated fast directions associated with the proposed EDC should mostly be NW–SE, which is almost orthogonal to the observed fast directions which are dominantly NE–SW along the northern edge of the craton and in the CVL (Fig. 6).

Another possible locale for EDC is the boundary between the Congo craton and the Atlantic Ocean basin with a nearly E–W flow direction (Reusch et al., 2010; Koch et al., 2012; Milelli et al., 2012). This EDC system, if exists, should produce a volcanic line in the Atlantic Ocean that is parallel to the western edge of the Congo craton with a N–S strike, which is not observed. Thus EDC cannot be responsible for the seismic anisotropy observed beneath the continental or the oceanic section of the CVL.

6.5. APM induced anisotropy

Numerous studies have suggested that simple shear at the base of the plate can lead to LPO oriented in the direction of shear beneath plates that move at velocities significantly different from those of the deep convection (e.g., Zhang and Karato, 1995; Tommasi et al., 1996; Tommasi, 1998; Walker et al., 2004; Liu, 2009; Barruol and Fontaine, 2013). As a result, a model that involves asthenospheric flow induced by a moving plate is used to account for large-scale uniform anisotropy with fast directions that are parallel to the APM (e.g., Vinnik et al., 1989; Walker et al., 2004; Marone and Romanowicz, 2007; Liu, 2009). However, the assumption of a positive relationship between fast directions and APM may not hold true for plates that move at small velocities relative to the underlain asthenosphere.

The APM for the African plate is small, which is partially responsible for the poorly constrained plate motion directions (e.g., Walker et al., 2004; Barruol and Fontaine, 2013). The current APM direction of the study area based on the HS3-NUVEL1A hot-spot model (Gripp and Gordon, 2002) is approximately toward the west (260°) (Fig. 1), with a rate of 1.7 cm/yr. The majority of the observed fast directions in the vicinity of the CVL (Figs. 1 and 6) are at a high angle (>30°) with the APM direction predicted by the HS3-NUVEL1A model. The GMHRF model (Dobrovine et al., 2012) predicts that the present-day motion of Africa is ENE (68°) at a rate of 1.3 cm/yr (Fig. 1). The spatially varying fast directions and the large misfit between the fast directions and the APM direction from either of the models in the study area (Figs. 1 and 6) suggest that APM-induced fabrics beneath slow-moving plates such as Africa may not be a major contribution to the observed anisotropy.

6.6. Mantle flow in a lithospheric channel

The dominantly CVL-parallel fast directions can be explained by NE-ward (relative to the lithosphere) mantle flow along a lithospheric channel beneath the CVL (Fig. 8A). Recent mantle flow

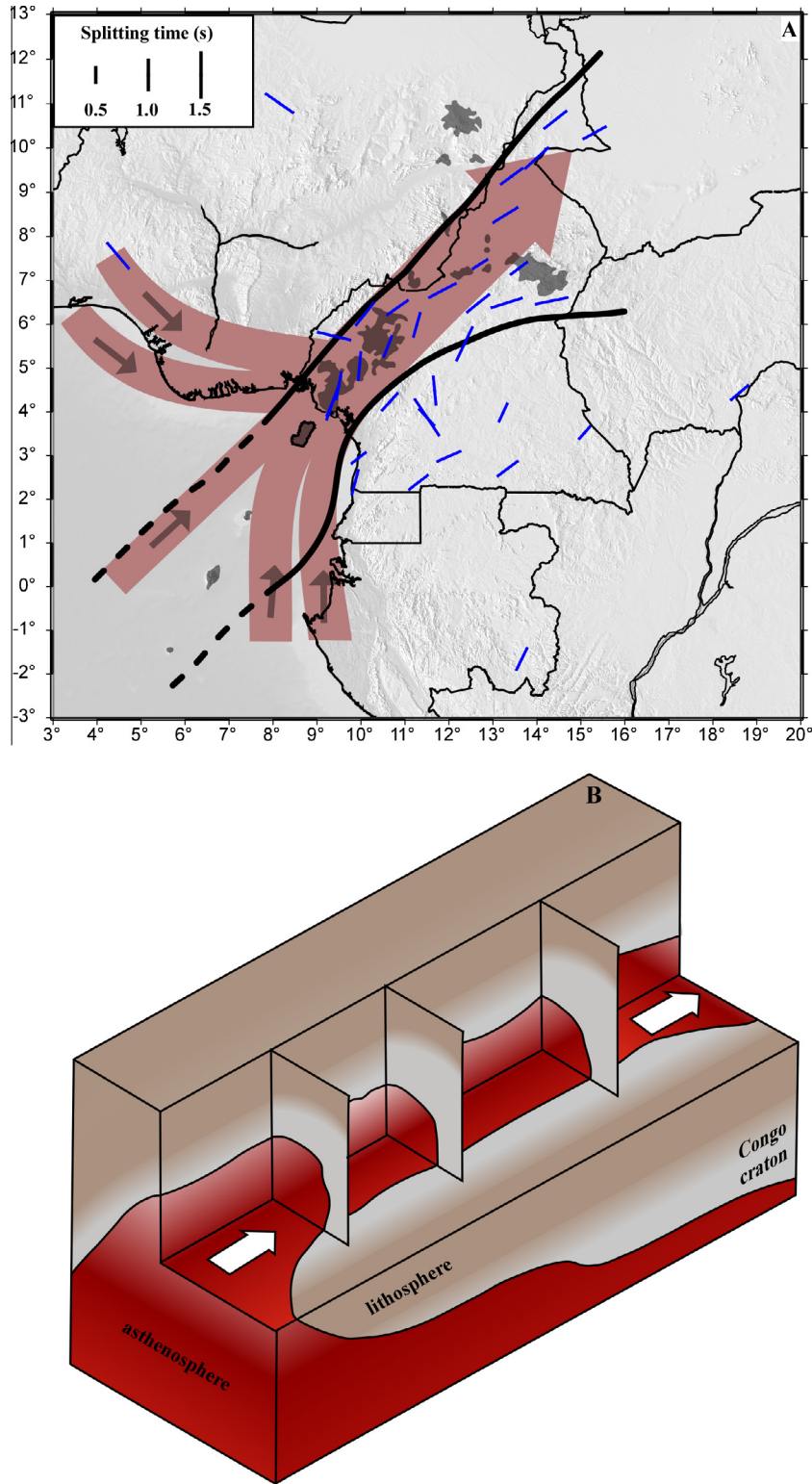


Fig. 8. (A). A map view of the study area showing station-averaged XKS splitting parameters (blue bars) and proposed mantle flow lines (brown bands with arrows). (B). A schematic Three-dimensional perspective view illustrates how the asthenospheric material flows along the base of the CVL continental lithosphere. (For interpretation of the references to color in this figure legend, the reader is referred to the web version of this article.)

models suggest that the lithosphere in the study areas is underlain by a NE (relative to the lithosphere) directed flow (Conrad and Behn, 2010; Forte et al., 2010). Forte et al. (2010) studied the mantle flow field at the depth of 250 km using the joint inversion of mantle rheological structure and density perturbations. Forte

et al. (2010) suggested that the asthenosphere is moving toward the NE with a velocity of 5.0 cm/yr beneath the CVL and the neighboring regions (Fig. 1). In addition, most seismic tomographic studies of the upper mantle clearly show the existence of low-velocity anomalies beneath the CVL relative to the bordering cratons/

shields (e.g., King and Ritsema, 2000; Reusch et al., 2010). Reusch et al. (2010) used data recorded by the CBSE network to study the upper mantle structure beneath the CVL. They found a tabular, low-velocity anomaly underlying both the continental and oceanic sections of the CVL with a depth that extends to ~300 km (Fig. 6).

We propose that the flow is driven by the SW movements of the lithosphere relative to the asthenosphere, and the direction of the flow is modulated by the geometry of the channel (Fig. 8), resulting in fast directions that are dominantly parallel to the CVL for measurements with ray-piercing points beneath the CVL. Under this model, stations adjacent to the CVL but with non-CVL-parallel fast directions such as CM20 (Fig. 2) and those in Area B (Fig. 3) could be interpreted as being located near the northern and southern boundaries, respectively, of the lithospheric channel (Fig. 6). Additionally, the coast-parallel fast directions observed at stations on the Nigerian shield could be explained as reflecting the flow deflected by the keel of the African continent. Such a deflection was suggested beneath the western (Refayee et al., 2013) and southern (Fouch et al., 2000; Gao et al., 2008) edges of the North American craton.

6.7. Implications on the formation of the CVL

As detailed above, in spite of numerous geochemical, geophysical, and geodynamic investigations, the formation of the CVL remains enigmatic. The lack of a clear age progression of the volcanoes in the CVL and the isotopic signatures ruled out a plume origin of both the continental and oceanic sections of the CVL. Edge-driven small-scale mantle convection cannot explain the orientation of the CVL or the formation of its oceanic section. Viable hypotheses for its formation should be able to explain the linearity, orientation, location, lack of age progression, and possibly its upper-mantle origin (as indicated by isotopic studies) of the volcanic line. In this section, we propose a hypothesis for the formation of the CVL that can explain most, if not all, of previous observations as well as our new shear-wave splitting measurements. This hypothesis is based on recent geodynamic modeling results suggesting the possibility of thermal–mechanical erosion of the base of the lithosphere by concentrated asthenospheric flow (Davies, 1994; Ribe and Christensen, 1994; Sleep, 1994; Artemieva and Mooney, 2002; Conrad et al., 2011). We propose that the CVL was developed by gradual basal erosion of the underlying lithosphere, along a line with the maximum flow intensity originated from the 90° sharp change in the orientation of the western margin of central Africa, from E–W north of the CVL to N–S south of the CVL (Fig. 2).

This hypothesis can explain one of the puzzling features of the CVL, i.e., it intercepts the African coastline exactly at the joint point between the E–W and N–S segments of the coastline, and forms a nearly 45° angle with both segments (Fig. 8). We suggest that the 90° turn of the continental margin creates a perfect locale for the concentration of mantle flow that originates from the SW-ward movement (relative to the asthenosphere) of the African lithosphere and is deflected by the cratonic keel (Fig. 8A). Such a relative movement is suggested by geodynamic modeling (Forte et al., 2010) (Fig. 1). Beneath the Atlantic Ocean, the flow concentration extends toward the SW with a gradually decreasing intensity and produces the oceanic section of the CVL. This interpretation is consistent with the SW-ward decrease of the size of the volcanoes on the ocean floor (Fig. 8A). It is also consistent with the suggestion that there is a low-velocity zone beneath the Principe Island (Meyers et al., 1998) and beneath the rest of the oceanic section of the CVL (Reusch et al., 2010).

This model suggests that the source of magma is at the base of the thinned lithosphere which is consistent with isotopic observations (e.g., Aka et al., 2004). According to this hypothesis, the lack

of age progression of the eruptions can be explained by the fact that volcanic eruptions took place in areas with the maximum lithospheric thinning, which is controlled by pre-existing zones of weakness and the distribution of mechanical strength in the lithosphere.

7. Conclusions

The CVL and the adjacent areas are tectonically complex regions which includes cratons, mobile belts, and shear zones, and active magmatism. Our SWS results suggest that the anisotropy beneath the CVL and surrounding areas is mostly located in the asthenosphere, although fossilized anisotropy in the northern part of the Congo craton cannot be ruled out. Spatial distribution of the splitting parameters in the study area does not support the small-scale mantle convection hypothesis nor the mantle plume and APM models as a cause for the observed anisotropy. We suggest that the predominant NE oriented anisotropy beneath the CVL is from a NE-ward (relative to the lithosphere) mantle flow along a lithospheric channel beneath the CVL. This channel is developed due to the differential movement of the African plate relative to the underlying asthenosphere as suggested by several geodynamic modeling studies. The model attributes coast-parallel fast directions north of the CVL to mantle flow deflected by the edge of the Africa continent keel. We suggest that the flood basalts along the CVL were formed by gradual basal erosion of the lithosphere, as a result of concentration of mantle flow associated with the sharp change in the orientation of the continental margin of western Africa. Additional shear-wave splitting and other measurements in the coastal areas and on the ocean floor in the vicinity of the CVL should be able to test and refine the proposed hypothesis.

Acknowledgments

We thank the participants of the CBSE and the IRIS DMC for providing the high-quality seismic data used in the study. We also thank C. Conrad and A. Forte for providing mantle flow modeling results and A. Mohamed for helping with illustrating Fig. 8B. We are grateful to H. Al-Doukhi and R. Haselwander for discussions. We thank the Associate Editor and two anonymous reviewers for their constructive comments and suggestions. The work was partially supported by NSF award EAR-1009946.

References

- Abdelsalam, M.G., Gao, S.S., Liégeois, J.-P., 2011. Upper mantle structure of the Saharan Metacraton. *J. Afr. Earth Sc.* 60, 328–336. <http://dx.doi.org/10.1016/j.jafrearsci.2011.03.009>.
- Aka, F.T., Nagao, K., Kusakabe, M., Sumino, H., Tanyileke, G., Ateba, B., Hell, J., 2004. Symmetrical Helium isotope distribution on the Cameroon Volcanic Line, West Africa. *Chem. Geol.* 203, 205–223. <http://dx.doi.org/10.1016/j.chemgeo.2003.10.003>.
- Anderson, D.L., 1994. The sublithospheric mantle as the source of continental flood basalts; the case against the continental lithosphere and plume head reservoirs. *Earth Planet. Sci. Lett.* 123, 269–280. [http://dx.doi.org/10.1016/0012-821X\(94\)90273-9](http://dx.doi.org/10.1016/0012-821X(94)90273-9).
- Anderson, D.L., 2000. The thermal state of the upper mantle; No role for mantle plumes. *Geophys. Res. Lett.* 27, 3623–3626. <http://dx.doi.org/10.1029/2000GL011533>.
- Anderson, D.L., 2001. Top-down tectonics? *Science* 293, 2016–2018.
- Artemieva, I.M., Mooney, W.D., 2002. On the relations between cratonic lithosphere thickness, plate motions, and basal drag. *Tectonophysics* 358, 211–231. [http://dx.doi.org/10.1016/S0040-1951\(02\)00425-0](http://dx.doi.org/10.1016/S0040-1951(02)00425-0).
- Babuška, V., Plomerová, J., 1989. Seismic Anisotropy of the Subcrustal Lithosphere in Europe: Another Clue to Recognition of Accreted Terranes. *AGU, Washington, DC*, pp. 209–217.
- Bagley, B., Nyblade, A.A., 2013. Seismic anisotropy in eastern Africa, mantle flow, and the African superplume. *Geophys. Res. Lett.* 40, 1500–1505. <http://dx.doi.org/10.1002/grl.50315>.

- Barruol, G., Fontaine, F.R., 2013. Mantle flow beneath La Réunion hotspot track from SKS splitting. *Earth Planet. Sci. Lett.* 362, 108–121. <http://dx.doi.org/10.1016/j.epsl.2012.11.017>.
- Barruol, G., Hoffmann, R., 1999. Upper mantle anisotropy beneath the Geoscope stations. *J. Geophys. Res.: Solid Earth* 104, 10757–10773. <http://dx.doi.org/10.1029/1999JB900033>.
- Barruol, G., Ismail, W.B., 2001. Upper mantle anisotropy beneath the African IRIS and geoscope stations. *Geophys. J. Int.* 146, 549–561. <http://dx.doi.org/10.1046/j.0956-540x.2001.01481.x>.
- Bastow, I.D., Keir, D., 2011. The protracted development of the continent-ocean transition in Afar. *Nat. Geosci.* 4, 248–250. <http://dx.doi.org/10.1038/ngeo1095>.
- Begg, G.C., Griffin, W.L., Natapov, L.M., O'Reilly, S.Y., Grand, S.P., O'Neill, C.J., Hronsky, J.M.A., Djomani, Y.P., Swain, C.J., Deen, T., Bowden, P., 2009. The lithospheric architecture of Africa: seismic tomography, mantle petrology, and tectonic evolution. *Geosphere* 5, 23–50.
- Birch, F., 1960. The velocity of compressional waves in rocks to 10 kilobars: 1. *J. Geophys. Res.* 65, 1083–1102. <http://dx.doi.org/10.1029/JZ065i004p01083>.
- Burke, K., 2001. Origin of the Cameroon Line of Volcano-capped swells. *J. Geol.* 109, 349–362. <http://www.jstor.org/stable/10.1086/319977>.
- Burke, K., Dewey, J.F., 1973. Plume-generated triple junctions: key indicators in applying plate tectonics to old rocks. *J. Geol.* 81, 406–433.
- Castaing, C., Feybesse, J.L., Thiéblemont, D., Triboulet, C., Chèvremont, P., 1994. Palaeogeographical reconstructions of the Pan-African/Brasiliano orogen: closure of an oceanic domain or intracontinental convergence between major blocks? *Precamb. Res.* 69, 327–344. [http://dx.doi.org/10.1016/0301-9268\(94\)90095-7](http://dx.doi.org/10.1016/0301-9268(94)90095-7).
- Chastel, Y.B., Dawson, P.R., Wenk, H.-R., Bennett, K., 1993. Anisotropic convection with implications for the upper mantle. *J. Geophys. Res.: Solid Earth* 98, 17757–17771. <http://dx.doi.org/10.1029/93JB01161>.
- Chevrot, S., 2000. Multichannel analysis of shear wave splitting. *J. Geophys. Res.: Solid Earth* 105, 21579–21590. <http://dx.doi.org/10.1029/2000JB900199>.
- Conrad, C.P., Behn, M.D., 2010. Constraints on lithosphere net rotation and seismic asthenospheric viscosity from global mantle flow models and seismic anisotropy. *Geochem. Geophys. Geosyst.* 11, 1–19. <http://dx.doi.org/10.1029/2009GC002970>.
- Conrad, C.P., Behn, M.D., Silver, P.G., 2007. Global mantle flow and the development of seismic anisotropy: differences between the oceanic and continental upper mantle. *J. Geophys. Res.: Solid Earth* 112, B07317. <http://dx.doi.org/10.1029/2006JB004608>.
- Conrad, C.P., Bianco, T.A., Smith, E.I., Wessel, P., 2011. Patterns of intraplate volcanism controlled by asthenospheric shear. *Nat. Geosci.* 4, 317–321. <http://dx.doi.org/10.1038/ngeo1111>.
- Courtillot, V., Davaile, A., Besse, J., Stock, J., 2003. Three distinct types of hotspots in the Earth's mantle. *Earth Planet. Sci. Lett.* 205, 295–308. [http://dx.doi.org/10.1016/S0012-821X\(02\)01048-8](http://dx.doi.org/10.1016/S0012-821X(02)01048-8).
- Davies, G.F., 1994. Thermomechanical erosion of the lithosphere by mantle plumes. *J. Geophys. Res.: Solid Earth* 99, 15709–15722. <http://dx.doi.org/10.1029/94JB00119>.
- De Plaen, R.S.M., Bastow, I.D., Chambers, E.L., Keir, D., Gallacher, R.J., Keane, J., 2014. The development of magmatism along the Cameroon Volcanic Line: evidence from seismicity and seismic anisotropy. *J. Geophys. Res.: Solid Earth*. <http://dx.doi.org/10.1002/2013jb010583>.
- Deruelle, B., Moreau, C., Nkoumbou, C., Kambou, R., Lissom, J., Njonfang, E., Ghogomu, R.T., Nono, A., 1991. The Cameroon Line: a review. In: Kampunzu, A.B., Lubala, R.T. (Eds.), *Magmatism in Extensional Structural Settings*. Springer, Berlin, Heidelberg, pp. 274–327. http://dx.doi.org/10.1007/978-3-642-73966-8_12.
- Deruelle, B., Ngounouno, I., Demaiffe, D., 2007. The 'Cameroon Hot Line' (CHL): a unique example of active alkaline intraplate structure in both oceanic and continental lithospheres. *C.R. Geosci.* 339, 589–600. <http://dx.doi.org/10.1016/j.crte.2007.07.007>.
- Djomani, Y.H.P., Nnange, J.M., Diamant, M., Ebinger, C.J., Fairhead, J.D., 1995. Effective elastic thickness and crustal thickness variations in west central Africa inferred from gravity data. *J. Geophys. Res.: Solid Earth* 100, 22047–22070. <http://dx.doi.org/10.1029/95JB01149>.
- Dorbath, C., Dorbath, L., Fairhead, J.D., Stuart, G.W., 1986. A teleseismic delay time study across the central African shear zone in the Adamawa region of Cameroon, west Africa. *Geophys. J. Roy. Astron. Soc.* 86 (3), 751–766. <http://dx.doi.org/10.1111/j.1365-246X.1986.tb00658.x>.
- Dobrovine, P.V., Steinberger, B., Torsvik, T.H., 2012. Absolute plate motions in a reference frame defined by moving hot spots in the Pacific, Atlantic, and Indian oceans. *J. Geophys. Res.: Solid Earth* 117, B09101. <http://dx.doi.org/10.1029/2011JB009072>.
- Druken, K.A., Kincaid, C., Griffiths, R.W., 2013. Directions of seismic anisotropy in laboratory models of mantle plumes. *Geophys. Res. Lett.* 40, 3544–3549. <http://dx.doi.org/10.1002/grl.50671>.
- Ebinger, C.J., Sleep, N.H., 1998. Cenozoic magmatism throughout east Africa resulting from impact of a single plume. *Nature* 395, 788–791. <http://dx.doi.org/10.1038/27417>.
- Elsheikh, A.A., Gao, S.S., Liu, K.H., Mohamed, A.A., Yu, Y., Fat-Helbary, R.E., 2014. Seismic anisotropy and subduction-induced mantle fabrics beneath the Arabian and Nubian Plates adjacent to the Red Sea. *Geophys. Res. Lett.* 41, 2376–2381.
- Fairhead, J.D., 1988. Mesozoic plate tectonic reconstructions of the central South Atlantic Ocean: the role of the West and Central African rift system. *Tectonophysics* 155, 181–191. [http://dx.doi.org/10.1016/0040-1951\(88\)90265-X](http://dx.doi.org/10.1016/0040-1951(88)90265-X).
- Fairhead, J.D., Okereke, C.S., 1987. A regional gravity study of the West African rift system in Nigeria and Cameroon and its tectonic interpretation. *Tectonophysics* 143, 141–159. [http://dx.doi.org/10.1016/0040-1951\(87\)90084-9](http://dx.doi.org/10.1016/0040-1951(87)90084-9).
- Fitton, J.G., 1987. The Cameroon line, West Africa: a comparison between oceanic and continental alkaline volcanism. *Geol. Soc., London, Spec. Publ.* 30, 273–291.
- Fitton, J.G., Dunlop, H.M., 1985. The Cameroon line, West Africa, and its bearing on the origin of oceanic and continental alkali basalt. *Earth Planet. Sci. Lett.* 72, 23–38. [http://dx.doi.org/10.1016/0012-821X\(85\)90114-1](http://dx.doi.org/10.1016/0012-821X(85)90114-1).
- Fitton, J.G., Hughes, D.J., 1981. Strontian melilite in nephelinite lava from Etinde. *Mineral. Mag.* 44, 261–264.
- Forste, A.M., Quéré, S., Moucha, R., Simmons, N.A., Grand, S.P., Mitrovica, J.X., Rowley, D.B., 2010. Joint seismic–geodynamic–mineral physical modelling of African geodynamics: a reconciliation of deep-mantle convection with surface geophysical constraints. *Earth Planet. Sci. Lett.* 295, 329–341. <http://dx.doi.org/10.1016/j.epsl.2010.03.017>.
- Fouch, M.J., Rondenay, S., 2006. Seismic anisotropy beneath stable continental interiors. *Phys. Earth Planet. Inter.* 158, 292–320. <http://dx.doi.org/10.1016/j.pepi.2006.03.024>.
- Fouch, M.J., Fischer, K.M., Parmentier, E.M., Wysession, M.E., Clarke, T.J., 2000. Shear wave splitting, continental keels, and patterns of mantle flow. *J. Geophys. Res.: Solid Earth* 105, 6255–6275. <http://dx.doi.org/10.1029/1999JB900372>.
- Fouch, M.J., Silver, P.G., Bell, D.R., Lee, J.N., 2004. Small-scale variations in seismic anisotropy near Kimberley, South Africa. *Geophys. J. Int.* 157, 764–774. <http://dx.doi.org/10.1111/j.1365-246X.2004.02234.x>.
- Gallacher, R.J., Bastow, I.D., 2012. The development of magmatism along the Cameroon Volcanic Line: evidence from teleseismic receiver functions. *Tectonics* 31, TC3018. <http://dx.doi.org/10.1029/2011TC003028>.
- Gao, S.S., Liu, K.H., 2009. Significant seismic anisotropy beneath the southern Lhasa Terrane, Tibetan Plateau. *Geochem. Geophys. Geosyst.* 10, Q02008. <http://dx.doi.org/10.1029/2008GC002227>.
- Gao, S., Davis, P.M., Liu, H., Slack, P.D., Zorin, Y.A., Mordvinova, V.V., Kozhevnikov, V.M., Meyer, R.P., 1994. Seismic anisotropy and mantle flow beneath the Baikal rift zone. *Nature* 371, 149–151. <http://dx.doi.org/10.1038/371149a0>.
- Gao, S., Davis, P.M., Liu, H., Slack, P.D., Rigor, A.W., Zorin, Y.A., Mordvinova, V.V., Kozhevnikov, V.M., Logatchev, N.A., 1997. SKS splitting beneath continental rift zones. *J. Geophys. Res.: Solid Earth* 102, 22781–22797. <http://dx.doi.org/10.1029/97JB01858>.
- Gao, S.S., Liu, K.H., Stern, R.J., Keller, G.R., Hogan, J.P., Pulliam, J., Anthony, E.Y., 2008. Characteristics of mantle fabrics beneath the south-central United States: constraints from shear-wave splitting measurements. *Geosphere* 4, 411–417.
- Gao, S.S., Liu, K.H., Abdelsalam, M.G., 2010. Seismic anisotropy beneath the Afar Depression and adjacent areas: implications for mantle flow. *J. Geophys. Res.: Solid Earth* 115, B12330. <http://dx.doi.org/10.1029/2009JB007141>.
- Gashawbeza, E.M., Klemperer, S.L., Nyblade, A.A., Walker, K.T., Keranen, K.M., 2004. Shear-wave splitting in Ethiopia: Precambrian mantle anisotropy locally modified by Neogene rifting. *Geophys. Res. Lett.* 31, L18602. <http://dx.doi.org/10.1029/2009JB007141>.
- Gripp, A.E., Gordon, R.G., 2002. Young tracks of hotspots and current plate velocities. *Geophys. J. Int.* 150, 321–361. <http://dx.doi.org/10.1046/j.1365-246X.2002.01627.x>.
- Hansen, S.E., Nyblade, A.A., Julià, J., 2009. Estimates of crustal and lithospheric thickness in Sub-Saharan Africa from S-wave receiver functions. *S. Afr. J. Geol.* 112, 229–240.
- CGMW and UNESCO 1990. International Geological Map of Africa.
- James, D.E., Assumpcao, M., 1996. Tectonic implications of S-wave anisotropy beneath SE Brazil. *Geophys. J. Int.* 126, 1–10.
- Karato, S.C., Jung, H., Katayama, I., Skemer, P., 2008. Geodynamic significance of seismic anisotropy of the upper mantle: new insights from laboratory studies. *Annu. Rev. Earth Planet. Sci.* 36, 59–95. <http://dx.doi.org/10.1146/annurev.earth.36.031207.124120>.
- Kendall, J.M., Stuart, G.W., Ebinger, C.J., Bastow, I.D., Keir, D., 2005. Magma-assisted rifting in Ethiopia. *Nature* 433, 146–148. <http://dx.doi.org/10.1038/nature03161>.
- Kendall, J.M., Piliidou, S., Keir, D., Bastow, I.D., Stuart, G.W., Ayele, A., 2006. Mantle upwellings, melt migration and the rifting of Africa: insights from seismic anisotropy. *Geol. Soc., London, Spec. Publ.* 259, 55–72. <http://dx.doi.org/10.1144/gsl.sp.2006.259.01.06>.
- King, S.D., 2007. Hotspots and edge-driven convection. *Geology* 35, 223–226.
- King, S.D., Anderson, D.L., 1995. An alternative mechanism of flood basalt formation. *Earth Planet. Sci. Lett.* 136, 269–279. [http://dx.doi.org/10.1016/0012-821X\(95\)00205-Q](http://dx.doi.org/10.1016/0012-821X(95)00205-Q).
- King, S.D., Anderson, D.L., 1998. Edge-driven convection. *Earth Planet. Sci. Lett.* 160, 289–296. [http://dx.doi.org/10.1016/S0012-821X\(98\)00089-2](http://dx.doi.org/10.1016/S0012-821X(98)00089-2).
- King, S.D., Ritsema, J., 2000. African Hot Spot Volcanism: small-scale convection in the upper mantle beneath cratons. *Science* 290, 1137–1140. <http://dx.doi.org/10.1126/science.290.5494.1137>.
- Koch, F.W., Wiens, D.A., Nyblade, A.A., Shore, P.J., Tibi, R., Ateba, B., Tabod, C.T., Nnange, J.M., 2012. Upper-mantle anisotropy beneath the Cameroon Volcanic Line and Congo Craton from shear wave splitting measurements. *Geophys. J. Int.* 190, 75–86. <http://dx.doi.org/10.1111/j.1365-246X.2012.05497.x>.
- Kreemer, C., 2009. Absolute plate motions constrained by shear wave splitting orientations with implications for hot spot motions and mantle flow. *J. Geophys. Res.: Solid Earth* 114, B10405. <http://dx.doi.org/10.1029/2009JB006416>.
- Lee, D.-C., Halliday, A.N., Fitton, J.G., Poli, G., 1994. Isotopic variations with distance and time in the volcanic islands of the Cameroon line: evidence for a mantle

- plume origin. *Earth Planet. Sci. Lett.* 123, 119–138. [http://dx.doi.org/10.1016/0012-821X\(94\)90262-3](http://dx.doi.org/10.1016/0012-821X(94)90262-3).
- Li, A., Chen, C., 2006. Shear wave splitting beneath the central Tien Shan and tectonic implications. *Geophys. Res. Lett.* 33, L22303. <http://dx.doi.org/10.1029/2006GL027717>.
- Liu, K.H., 2009. NA-SWS-1.1: a uniform database of teleseismic shear wave splitting measurements for North America. *Geochem. Geophys. Geosyst.* 10, Q05011. <http://dx.doi.org/10.1029/2009GC002440>.
- Liu, K.H., Gao, S.S., 2013. Making reliable shear-wave splitting measurements. *Bull. Seismol. Soc. Am.* 103, 2680–2693. <http://dx.doi.org/10.1785/0120120355>.
- Liu, H., Davis, P.M., Gao, S., 1995. SKS splitting beneath southern California. *Geophys. Res. Lett.* 22, 767–770. <http://dx.doi.org/10.1029/95GL00487>.
- Liu, K.H., Gao, S.S., Gao, Y., Wu, J., 2008. Shear wave splitting and mantle flow associated with the deflected Pacific slab beneath northeast Asia. *J. Geophys. Res.: Solid Earth* 113, B01305. <http://dx.doi.org/10.1029/2007JB005178>.
- Marone, F., Romanowicz, B., 2007. The depth distribution of azimuthal anisotropy in the continental upper mantle. *Nature* 447, 198–201. <http://dx.doi.org/10.1038/nature05742>.
- McKenzie, D., 1979. Finite deformation during fluid flow. *Geophys. J. Roy. Astron. Soc.* 58, 689–715. <http://dx.doi.org/10.1111/j.1365-246X.1979.tb04803.x>.
- McNamara, D.E., Owens, T.J., Silver, P.G., Wu, F.T., 1994. Shear wave anisotropy beneath the Tibetan Plateau. *J. Geophys. Res.: Solid Earth* 99, 13655–13665. <http://dx.doi.org/10.1029/93JB03406>.
- Meyers, J.B., Rosendahl, B.R., Harrison, C.G.A., Ding, Z.-D., 1998. Deep-imaging seismic and gravity results from the offshore Cameroon Volcanic Line, and speculation of African hotlines. *Tectonophysics* 284, 31–63. [http://dx.doi.org/10.1016/S0040-1951\(97\)00173-X](http://dx.doi.org/10.1016/S0040-1951(97)00173-X).
- Milelli, L., Fouré, L., Jaupart, C., 2012. A lithospheric instability origin for the Cameroon Volcanic Line. *Earth Planet. Sci. Lett.* 335–336, 80–87. <http://dx.doi.org/10.1016/j.epsl.2012.04.028>.
- Morgan, W.J., 1972. Deep mantle convection plumes and plate motions. *AAPG Bull.* 56, 203–213.
- Morgan, W.J., 1983. Hotspot tracks and the early rifting of the Atlantic. *Tectonophysics* 94, 123–139. [http://dx.doi.org/10.1016/0040-1951\(83\)90013-6](http://dx.doi.org/10.1016/0040-1951(83)90013-6).
- Nicolas, A., Christensen, N.I., 1987. Formation of anisotropy in upper mantle peridotites: a review, composition, structure and dynamics of the lithosphere–asthenosphere system. *Am. Geophys. Union* 16, 111–123. <http://dx.doi.org/10.1029/GD016p0111>.
- Nnange, J.M., Ngako, V., Fairhead, J.D., Ebinger, C.J., 2000. Depths to density discontinuities beneath the Adamawa Plateau region, Central Africa, from spectral analyses of new and existing gravity data. *J. Afr. Earth Sc.* 30, 887–901. [http://dx.doi.org/10.1016/S0899-5362\(00\)00058-0](http://dx.doi.org/10.1016/S0899-5362(00)00058-0).
- Nowacki, A., Wookey, J., Kendall, J.M., 2010. Deformation of the lowermost mantle from seismic anisotropy. *Nature* 467, 1091–1094. <http://dx.doi.org/10.1038/nature09507>.
- Nyblade, A.A., Robinson, S.W., 1994. The African Superswell. *Geophys. Res. Lett.* 21, 765–768. <http://dx.doi.org/10.1029/94GL00631>.
- Obrebski, M., Kiselev, S., Vinnik, L., Montagner, J.P., 2010. Anisotropic stratification beneath Africa from joint inversion of SKS and P receiver functions. *J. Geophys. Res.: Solid Earth* 115, B09313. <http://dx.doi.org/10.1029/2009JB006923>.
- Plomerova, J., Babuška, V., Dorbath, C., Dorbath, L., Lillie, R.J., 1993. Deep lithospheric structure across the Central African Shear Zone in Cameroon. *Geophys. J. Int.* 115, 381–390.
- Priestley, K., McKenzie, D., Debayle, E., Pilidou, S., 2008. The African upper mantle and its relationship to tectonics and surface geology. *Geophys. J. Int.* 175, 1108–1126. <http://dx.doi.org/10.1111/j.1365-246X.2008.03951.x>.
- Refayee, H.A., Yang, B.B., Liu, K.H., Gao, S.S., 2013. Mantle flow and lithosphere–asthenosphere coupling beneath the southwestern edge of the North American craton: constraints from shear-wave splitting measurements. *Earth Planet. Sci. Lett.* <http://dx.doi.org/10.1016/j.epsl.2013.01.031>.
- Reusch, A.M., Nyblade, A.A., Wiens, D.A., Shore, P.J., Ateba, B., Tabod, C.T., Nnange, J.M., 2010. Upper mantle structure beneath Cameroon from body wave tomography and the origin of the Cameroon Volcanic Line. *Geochem. Geophys. Geosyst.* 11, Q10W07. <http://dx.doi.org/10.1029/2010GC003200>.
- Reusch, A.M., Nyblade, A.A., Tibi, R., Wiens, D.A., Shore, P.J., Bekoa, A., Tabod, C.T., Nnange, J.M., 2011. Mantle transition zone thickness beneath Cameroon: evidence for an upper mantle origin for the Cameroon Volcanic Line. *Geophys. J. Int.* 187, 1146–1150. <http://dx.doi.org/10.1111/j.1365-246X.2011.05239.x>.
- Ribe, N.M., 1989. Seismic anisotropy and mantle flow. *J. Geophys. Res.: Solid Earth* 94, 213–4223. <http://dx.doi.org/10.1029/JB094iB04p04213>.
- Ribe, N.M., Christensen, U.R., 1994. Three-dimensional modeling of plume–lithosphere interaction. *J. Geophys. Res.: Solid Earth* 99, 669–682. <http://dx.doi.org/10.1029/93JB02386>.
- Ribe, N.M., Yu, Y., 1991. A theory for plastic deformation and textural evolution of olivine polycrystals. *J. Geophys. Res.: Solid Earth* 96, 8325–8335. <http://dx.doi.org/10.1029/90JB02721>.
- Ritsema, J., van Heijst, H., 2000. New seismic model of the upper mantle beneath Africa. *Geology* 28, 63–66.
- Sandvol, E., Seber, D., Calvert, A., Barazangi, M., 1998. Grid search modeling of receiver functions: implications for crustal structure in the Middle East and North Africa. *J. Geophys. Res.: Solid Earth* 103, 26899–26917. <http://dx.doi.org/10.1029/98JB02238>.
- Savage, M.K., 1999. Seismic anisotropy and mantle deformation: what have we learned from shear wave splitting? *Rev. Geophys.* 37, 65–106. <http://dx.doi.org/10.1029/98RG02075>.
- Schlüter, T., 2006. *Geological Atlas of Africa: With Notes on Stratigraphy, Tectonics, Economic Geology, Geohazards and Geosites of Each Country*, second ed. Springer, New York.
- Silver, P.G., 1996. Seismic anisotropy beneath the continents: probing the depths of geology. *Annu. Rev. Earth Planet. Sci.* 24, 385–432. <http://dx.doi.org/10.1146/annurev.earth.24.1.385>.
- Silver, P.G., Chan, W.W., 1991. Shear wave splitting and subcontinental mantle deformation. *J. Geophys. Res.: Solid Earth* 96, 16429–16454. <http://dx.doi.org/10.1029/91JB00899>.
- Silver, P.G., Savage, M.K., 1994. The interpretation of shear-wave splitting parameters in the presence of two anisotropic layers. *Geophys. J. Int.* 119, 949–963. <http://dx.doi.org/10.1111/j.1365-246X.1994.tb04027.x>.
- Silver, P.G., Gao, S.S., Liu, K.H., 2001. Mantle deformation beneath southern Africa. *Geophys. Res. Lett.* 28, 2493–2496. <http://dx.doi.org/10.1029/2000GL012696>.
- Sleep, N.H., 1994. Lithospheric thinning by midplate mantle plumes and the thermal history of hot plume material ponded at sublithospheric depths. *J. Geophys. Res.: Solid Earth* 99, 9327–9343. <http://dx.doi.org/10.1029/94JB00240>.
- Stuart, G.W., Fairhead, J.D., Dorbath, L., Dorbath, C., 1985. A seismic refraction study of the crustal structure associated with the Adamawa Plateau and Garoua Rift, Cameroon, West Africa. *Geophys. J. Int.* 81, 1–12.
- Tabod, C.T., Fairhead, J.D., Stuart, G.W., Ateba, B., Ntepe, N., 1992. Seismicity of the Cameroon Volcanic Line, 1982–1990. *Tectonophysics* 212, 303–320. [http://dx.doi.org/10.1016/0040-1951\(92\)90297-J](http://dx.doi.org/10.1016/0040-1951(92)90297-J).
- Tadjou, J.M., Nouayou, R., Kamguia, J., Kande, H.L., 2009. Gravity analysis of the boundary between the Congo craton and the Pan-African belt of Cameroon. *Austrian J. Earth Sci.* 102, 71–79.
- Tokam, A.-P.K., Tabod, C.T., Nyblade, A.A., Julià, J., Wiens, D.A., Pasyanos, M.E., 2010. Structure of the crust beneath Cameroon, West Africa, from the joint inversion of Rayleigh wave group velocities and receiver functions. *Geophys. J. Int.* 183, 1061–1076.
- Tommasi, A., 1998. Forward modeling of the development of seismic anisotropy in the upper mantle. *Earth Planet. Sci. Lett.* 160, 1–13. [http://dx.doi.org/10.1016/S0012-821X\(98\)00081-8](http://dx.doi.org/10.1016/S0012-821X(98)00081-8).
- Tommasi, A., Vauchez, A., Russo, R., 1996. Seismic anisotropy in ocean basins: resistive drag of the sublithospheric mantle? *Geophys. Res. Lett.* 23, 2991–2994. <http://dx.doi.org/10.1029/96GL02891>.
- Toteu, S.F., Penaye, J., Djomani, Y.P., 2004. U–Pb and Sm–Nd evidence for Eburnean and Pan-African high-grade metamorphism in cratonic rocks of southern Cameroon. *Can. J. Earth Sci.* 41, 73–85.
- Turcotte, D.L., Oxburgh, E.R., 1978. Intra-plate volcanism and discussion. *Philos. Trans. R. Soc. London. Ser. A: Math. Phys. Sci.* 288, 561–579.
- Van Houten, F.B., 1983. Sirte Basin, north-central Libya: cretaceous rifting above a fixed mantle hotspot? *Geology* 11, 115–118.
- Vauchez, A., Tommasi, A., Barruol, G., Maumun, J., 2000. Upper mantle deformation and seismic anisotropy in continental rifts. *Phys. Chem. Earth Part A* 25, 111–117. [http://dx.doi.org/10.1016/S1464-1895\(00\)00019-3](http://dx.doi.org/10.1016/S1464-1895(00)00019-3).
- Vinnik, L.P., Farra, V., Romanowicz, B., 1989. Azimuthal anisotropy in the Earth from observations of SKS at GEOSCOPE and NARS broadband stations. *Bull. Seismol. Soc. Am.* 79, 1542–1558.
- Walker, K.T., Bokelmann, G.H.R., Klemperer, S.L., 2001. Shear-wave splitting to test mantle deformation models around Hawaii. *Geophys. Res. Lett.* 28, 4319–4322. <http://dx.doi.org/10.1029/2001GL013299>.
- Walker, K.T., Nyblade, A.A., Klemperer, S.L., Bokelmann, G.H.R., Owens, T.J., 2004. On the relationship between extension and anisotropy: constraints from shear wave splitting across the East African Plateau. *J. Geophys. Res.: Solid Earth* 109, B08302. <http://dx.doi.org/10.1029/2003JB002866>.
- Walker, K.T., Bokelmann, G.H.R., Klemperer, S.L., Bock, G., 2005. Shear-wave splitting around the Eifel hotspot: evidence for a mantle upwelling. *Geophys. J. Int.* 163, 962–980.
- Wolfe, C.J., Solomon, S.C., 1998. Shear-wave splitting and implications for mantle flow beneath the MELT region of the East Pacific Rise. *Science* 280, 1230–1232.
- Zhang, S., Karato, S.I., 1995. Lattice preferred orientation of olivine aggregates deformed in simple shear. *Nature* 375, 774–777. <http://dx.doi.org/10.1038/375774a0>.
- Zhu, L., Kanamori, H., 2000. Moho depth variation in southern California from teleseismic receiver functions. *J. Geophys. Res.: Solid Earth* 105, 2969–2980. <http://dx.doi.org/10.1029/1999JB000322>.